



# Multivalent Siderophore–DOTAM Conjugates as Theranostics for Imaging and Treatment of Bacterial Infections

Kevin Ferreira<sup>+</sup>, Hai-Yu Hu<sup>+</sup>, Verena Fetz<sup>+</sup>, Hans Prochnow, Bushra Rais, Peter P. Müller, and Mark Brönstrup\*

**Abstract:** There is a strong need to better diagnose infections at deep body sites through noninvasive molecular imaging methods. Herein, we describe the synthesis and characterization of probes based on siderophore conjugates with catechol moieties and a central DOTAM scaffold. The probes can accommodate a metal ion as well as an antibiotic moiety and are therefore suited for theranostic purposes. The translocation of the conjugates across the outer and inner cell membranes of *E. coli* was confirmed by growth recovery experiments with enterobactin-deficient strains, by the antibacterial activity of ampicillin conjugates, and by confocal imaging using a fluorogen-activating protein–malachite green system adapted to *E. coli*. The suitability of the probes for *in vivo* imaging was demonstrated with a Cy5.5 conjugate in mice infected with *P. aeruginosa*.

Infections caused by pathogenic bacteria represent a major health threat that is expected to aggravate further in the future,<sup>[1]</sup> fueled by the facilitated spread of pathogens through international mobility and an increase in modern medical procedures that disrupt physical biological barriers and the immune system. The fact that a growing proportion of multidrug-resistant pathogens meet a declining pipeline of novel antibiotic drugs raises serious concerns. There is also a lack of methods to detect infections at sites that are unknown or inaccessible for sampling; this concerns in particular biomaterial-associated infections or endocarditis. For this purpose, noninvasive imaging methods that can detect early-stage infections are highly desirable as they would enable timely interventions before local manifestations

(e.g., through biofilm formation) or a systemic spread of the infection.<sup>[2]</sup>

The positron emission tomography (PET) agent 2-[<sup>18</sup>F]fluorodeoxyglucose (<sup>18</sup>F-FDG) is in clinical use, but cannot differentiate between sterile inflammation and bacterial infections. To address this issue, several probes for bacterial imaging have recently been published that are based on prothrombin,<sup>[3]</sup> maltodextrin,<sup>[4]</sup> sorbitol,<sup>[5]</sup> vancomycin, or substrates for the micrococcal nuclease (MN) and for the  $\beta$ -lactamases of *M. tuberculosis*.

Herein, we targeted the bacterial iron transport machinery to monitor and treat infections. To satisfy their iron demand, bacteria biosynthesize and secrete siderophores, small molecules with a high affinity for iron that capture the metal from the environment, followed by an active uptake of the iron–siderophore complex.<sup>[6]</sup> Multiple transporters enable bacteria to import not only endogenous siderophores, but also so-called xenosiderophores, thereby guaranteeing iron supply even in the absence of the endogenous molecules.<sup>[6b]</sup> Various groups have exploited this property for the design of actively transported antibacterial conjugates of an antibiotic effector coupled to an iron-binding motif. Achieving reliable efficacy towards adapting bacterial populations is seen as a major challenge of this approach for treatment<sup>[7]</sup> and imaging<sup>[8]</sup> applications.

We searched for a small-molecule scaffold that enables bacterial imaging and treatment (i.e., theranostic)<sup>[9]</sup> applications at the same time by accommodating 1) an iron-binding motif, 2) variable imaging modalities, and 3) an optional effector antibiotic. The tetrapodal 1,4,7,10-tetraazacyclododecane-1,4,7,10-tetraacetic amide (DOTAM) moiety was selected<sup>[10]</sup> because it fulfills all functional requirements and has various advantages such as straightforward synthetic access, high solubility, low toxicity, and proven biocompatibility.<sup>[11]</sup> This scaffold has also been widely applied for the chelation of metals, a property that is utilized in Ln-based magnetic resonance imaging, <sup>68</sup>Ga- or <sup>64</sup>Cu-based nuclear imaging, and <sup>90</sup>Y-based radiotherapy.<sup>[12]</sup>

For siderophore-based bacterial imaging, three of the four arms branching from the DOTAM core were functionalized with catechol moieties for iron binding while the fourth arm was coupled to a fluorophore through various linkers (Figure 1a). The imaging probes, antibiotics, and control compounds **1–13** were prepared in three to eight steps from cyclen (Scheme 1; see also the Supporting Information, Schemes S1–S7). The iron-binding properties of the compounds were determined by a colorimetric titration assay based on chrome azurol S (CAS).<sup>[13]</sup> Whereas **1** bound one equivalent of ferric

[\*] M. Sc. K. Ferreira,<sup>[+]</sup> Dr. H.-Y. Hu,<sup>[+]</sup> Dr. V. Fetz,<sup>[+]</sup> Dr. H. Prochnow, Dr. B. Rais, Prof. Dr. P. P. Müller, Prof. Dr. M. Brönstrup  
Department of Chemical Biology  
Helmholtz Centre for Infection Research and German Centre for Infection Research (DZIF)  
Inhoffenstrasse 7, 38124 Braunschweig (Germany)  
E-mail: mark.broenstrup@helmholtz-hzi.de

Dr. H.-Y. Hu<sup>[+]</sup>

State Key Laboratory of Bioactive Substances and Function of Natural Medicine, Institute of Materia Medica, Chinese Academy of Medical Sciences and Peking Union Medical College  
1 Xiannongtan Street, 100050 (P.R. China)

Dr. V. Fetz<sup>[+]</sup>

School of Engineering and Science  
Jacobs University Bremen (Germany)

[+] These authors contributed equally to this work.

Supporting information and the ORCID identification number(s) for the author(s) of this article can be found under:  
 <https://doi.org/10.1002/anie.201701358>.

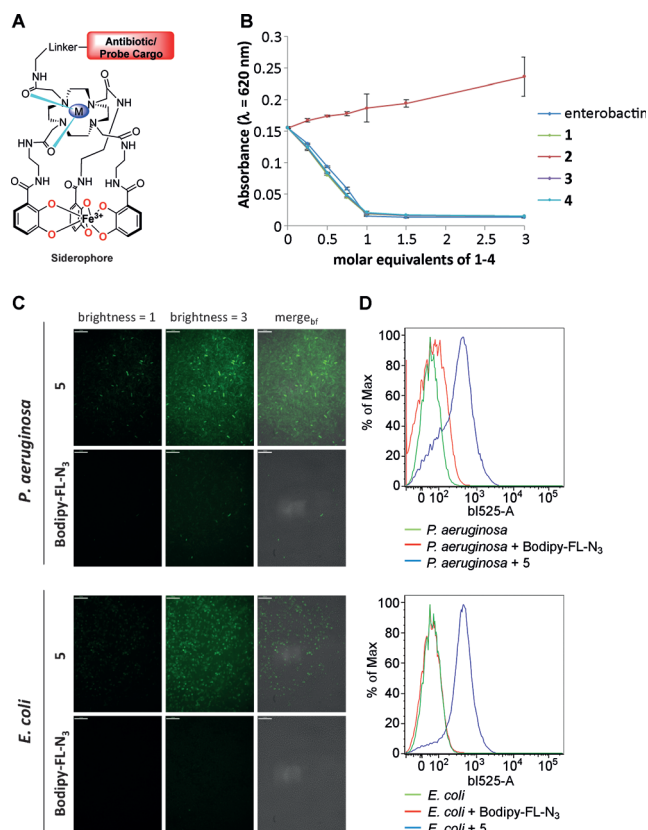


**Figure 1.** Binding properties of the siderophore conjugates. a) General structure of the conjugates. b) Iron-binding assays using CAS with 1–4 and enterobactin. c, d) Labeling of *P. aeruginosa* and *E. coli* with DOTAM–BODIPY conjugates or free BODIPY monitored by confocal microscopy (c) and flow cytometry (d). Scale bars: 11  $\mu$ m.

iron, no binding was observed for **2**, a complex that lacks free hydroxy groups for iron binding (Figure 1b).

This result suggests that ferric iron was indeed complexed by the catechol groups, and not by the DOTAM moiety. Comparison with **3** demonstrates that the modification of the

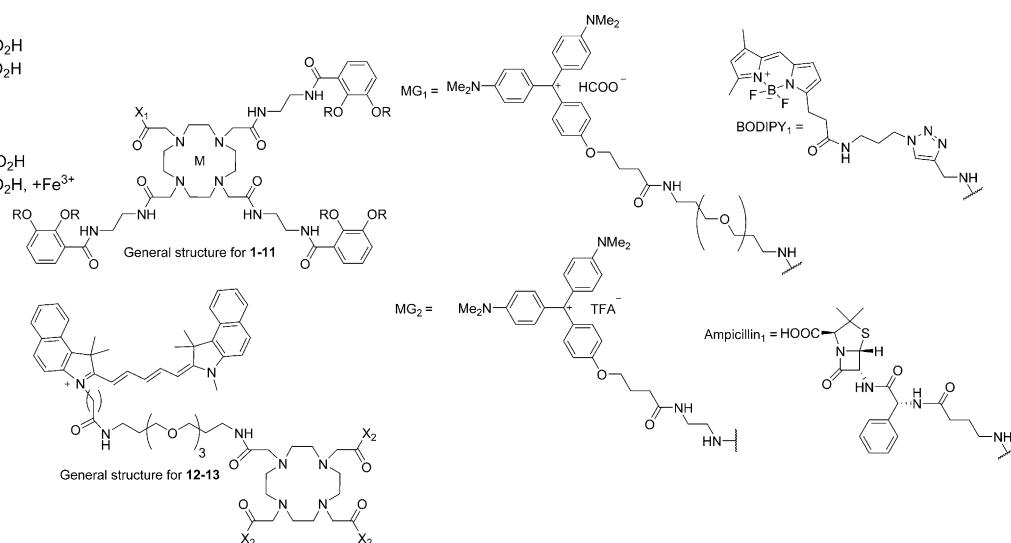
fourth arm with a GABA linker had no influence on binding. To probe whether a metal complexed to DOTAM would interfere with iron binding, the  $\text{Eu}^{3+}$ -containing complex **4** was titrated into an Fe/CAS solution. Again, one equivalent of ferric iron was found to bind to **4**, indicating that the scaffold can accommodate  $\text{Fe}^{3+}$  and  $\text{Eu}^{3+}$  simultaneously. Next, the ability of the DOTAM conjugates to label medically important bacterial pathogens of the ESKAPE panel, comprising the Gram-negative species *A. baumannii*, *E. cloacae*, *E. coli*, *K. pneumoniae*, and *P. aeruginosa* as well as the Gram-positive species *E. faecium* and *S. aureus*,<sup>[1c]</sup> was probed using **5**, a conjugate with a BODIPY fluorophore. All ESKAPE pathogens were labeled by **5** according to confocal microscopy and flow-cytometry experiments (Figures 1 and S1). However, we observed varying staining efficiencies between the strains, and in many cases, only a subpopulation of a given strain was labeled. This might be due to the different growth phases of the respective cells, but the molecular mechanism behind this finding remains unknown at this stage.

An important mechanistic question concerns the cellular localization of the DOTAM conjugates, that is, whether they bind to the outside of bacterial cells or are internalized by siderophore transporters. We addressed this issue by three sets of experiments based on growth recovery, antibacterial activity, and bacterial imaging.

First, the internalization of **1** and **6** into *E. coli* and *P. aeruginosa* cells was assessed by growth recovery assays with the mutants *E. coli*  $\Delta$ entA and *P. aeruginosa*  $\Delta$ pvd/ $\Delta$ pch. These strains cannot biosynthesize endogenous siderophores and therefore require the presence of exogenous siderophores to grow under iron-limiting conditions. Indeed, the growth of the *E. coli* and *P. aeruginosa* mutants was restored by the addition of the respective endogenous siderophores enterobactin and pyoverdine (Figure 2). Notably, the DOTAM-based siderophore mimics **1** (with free catechols) and **6** (with acetylated catechols) also promoted the growth of the mutant strains. In contrast, **2** (with benzylated catechols) failed to restore the growth of siderophore-deficient strains. These

- 1  $M = \text{I}$ ,  $R = \text{H}$ ,  $X_1 = \text{NH}(\text{CH}_2)_3\text{CO}_2\text{H}$
- 2  $M = \text{I}$ ,  $R = \text{Bn}$ ,  $X_1 = \text{NH}(\text{CH}_2)_3\text{CO}_2\text{H}$
- 3  $M = \text{I}$ ,  $R = \text{H}$ ,  $X_1 = \text{OH}$
- 4  $M = \text{Eu}^{3+}$ ,  $R = \text{H}$ ,  $X_1 = \text{OH}$
- 5  $M = \text{Zn}^{2+}$ ,  $R = \text{Ac}$ ,  $X_1 = \text{BODIPY}_1$
- 6  $M = \text{I}$ ,  $R = \text{Ac}$ ,  $X_1 = \text{NH}(\text{CH}_2)_3\text{CO}_2\text{H}$
- 7  $M = \text{I}$ ,  $R = \text{H}$ ,  $X_1 = \text{NH}(\text{CH}_2)_3\text{CO}_2\text{H}$ ,  $+\text{Fe}^{3+}$
- 8  $M = \text{I}$ ,  $R = \text{Ac}$ ,  $X_1 = \text{Ampicillin}_1$
- 9  $M = \text{Cu}^{2+}$ ,  $R = \text{Ac}$ ,  $X_1 = \text{Ampicillin}_1$
- 10  $M = \text{I}$ ,  $R = \text{Bn}$ ,  $X_1 = \text{MG}_1$
- 11  $M = \text{I}$ ,  $R = \text{Ac}$ ,  $X_1 = \text{MG}_2$

- 12  $X_2 = \text{NH}(\text{CH}_2)_3\text{CO}_2\text{H}$
- 13  $X_2 = \text{OH}$



**Scheme 1.** DOTAM-based siderophore conjugates used in this study.

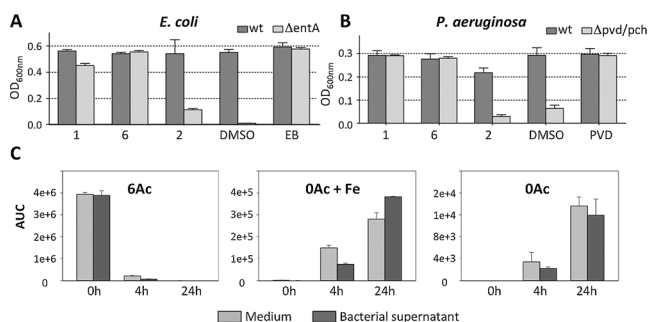


**Figure 2.** Growth recovery experiments and analysis of acetylation status. a) The growth of *E. coli* BW25113 (wt) and the enterobactin-deficient strain ( $\Delta$ entA) was assessed 48 h after compound addition. b) The growth of the *P. aeruginosa* strain PAO1 (wt) and the pyoverdine/pyochelin-deficient strains ( $\Delta$ pvdF/ $\Delta$ pvdA) was assessed 24 h after compound addition. All values are OD<sub>600</sub> measurements,  $n=2$ ,  $\pm$  SEM. c) Relative quantification of deacetylation and iron complexation of **6**. Compound **6** was incubated in LB medium at a final concentration of 10  $\mu$ M with (black bars) or without *E. coli*  $\Delta$ entB (gray bars), extracted at the indicated time points, and quantified by LC-MS/MS. Area under the curve (AUC) values represent the abundance of the monitored molecule and are shown for **6** (with 6 acetyl groups: 6Ac, left), **1** in complex with iron (0 acetyl groups: 0Ac + Fe, middle), and **1** (0 acetyl groups: 0Ac, right). Ac=acetyl, EB=enterobactin, PVD=pyoverdine.

experiments provide evidence that the DOTAM catecholates are indeed capable of delivering iron into Gram-negative bacteria through internalization. We employed acetylated catechols because the use of an acetyl prodrug that is activated in situ has been reported to be favorable to prevent the permanent inactivation of catecholates by enzymatic methylation.<sup>[7f,14]</sup>

To confirm that **6** can be deacetylated and complexed with iron, the relative abundances of the DOTAM catecholates carrying six or zero acetyl groups as well as the iron-complexed, deacetylated species **7** were determined by LC/MS/MS (Figures 2c and S2 and Table S1). We indeed observed full deacetylation and iron complexation; to our surprise, deacetylation occurred independent of bacterial hydrolases, as equal amounts of **1** were formed upon incubation in plain medium or with *E. coli*  $\Delta$ entB (Figure 2c).

Next, the  $\beta$ -lactam antibiotic ampicillin was coupled to the DOTAM core via a covalent, non-cleavable linker in six steps to give **8** with an overall yield of 15% (Scheme S5). Conjugate **8** inhibited the growth of the enterobactin-deficient strains *E. coli*  $\Delta$ entA and *E. coli*  $\Delta$ entB and the enterobactin-receptor-deficient strain *E. coli*  $\Delta$ fepA with IC<sub>50</sub> values comparable to those of free ampicillin (Table 1). The enhanced activity of **8** on the enterobactin-deficient mutants compared to the wild type implies that the DOTAM core is

**Table 1:** Growth inhibition activities (IC<sub>50</sub>) of the DOTAM conjugates and free ampicillin in  $\mu$ M.

Compound	<i>E. coli</i>	$\Delta$ entA	$\Delta$ entB	$\Delta$ fepA
<b>8</b>	30.2	2.1	3.3	7.2
<b>9</b>	> 50	1.9	2.1	> 50
ampicillin	4.3	2.1	6.2	3.8

accepted as an iron carrier, while the lack of activity on the wild type may reflect a saturation of the iron demand of the *E. coli* by its endogenous siderophore. The activity against FepA-deficient mutants demonstrates that **8** may also enter the bacterial cell through different transporters; this is seen as an advantage as it suggests that resistance cannot be induced by mutations or downregulation of a single target. The addition of Cu<sup>2+</sup> to yield **9** slightly improved the IC<sub>50</sub> value for *E. coli*  $\Delta$ entA and *E. coli*  $\Delta$ entB, but led to a decrease in activity for *E. coli* wt and  $\Delta$ fepA. As the targets of ampicillin are located in the periplasmic space, the antibiotic activity indicates a translocation of the conjugate at least through the outer membrane.

The question whether the DOTAM conjugates could pass through the inner membrane was investigated with a conjugate with the fluorogenic dye malachite green (MG). Whereas MG itself is not fluorescent, binding to the fluorogen activating protein (FAP), a 25 kDa single-chain antibody fragment, hinders rotation of the aromatic rings, thereby strongly enhancing the fluorescence of MG (Figures 3a and S4).<sup>[15]</sup> While a first adaptation of the FAP/MG system to the high-resolution imaging of prokaryotes has recently been reported,<sup>[16]</sup> we aimed at applying MG/FAP to study the translocation efficiencies of molecular scaffolds designed to transport cargos in bacteria. For this purpose, the sequence of variant FAP6.2 was cloned into the pET23b expression vector and recombinantly expressed in *E. coli* Origami™ B(DE3). FAP6.2 expression was confirmed by Western blot analysis and by monitoring the MG fluorescence upon incubation with purified FAP6.2 (Figure S4).

Whereas the incubation of *E. coli* *FAP6.2* with the MG-coupled, benzyl-protected DOTAM conjugate **10** did not induce fluorescence, incubation with **11** led to a time-dependent increase in fluorescence (Figure 3b). After 16 h of incubation, the MG-dependent fluorescence of the bacteria was further analyzed by flow cytometry and confocal microscopy (Figures 3b and S5). To exclude that an antibacterial effect of **11** caused the detected uptake kinetics, the bacteria were afterwards incubated with propidium iodide, a dye that specifically labels dead cells, and examined by confocal microscopy (Figure S6). We did not observe an enhanced amount of dead cells upon treatment with **11**, underlining the validity of uptake into live cells. As the observed fluorescence required the binding of intracellular FAP to DOTAM-conjugated MG, these findings provide evidence that **11** had indeed been translocated into the cytosol of *E. coli*.

Encouraged by the cellular imaging data, the ability of DOTAM-siderophore conjugates to monitor bacterial infections in vivo was probed with **12**, a conjugate that carries the near-infrared dye Cy5.5, which is compatible with the optical imaging of small animals. Interferon- $\beta$  luciferase reporter mice were infected subcutaneously with a nonlethal dose of *P. aeruginosa* or with a solvent control. Upon injection of **12** (20  $\mu$ g kg<sup>-1</sup>) into the tail vein, the fluorescence was monitored over 24 h (Figures 4a and S7). A second negative control group was infected with *P. aeruginosa* and then treated with the DOTA conjugate **13**, which is devoid of catechol moieties.

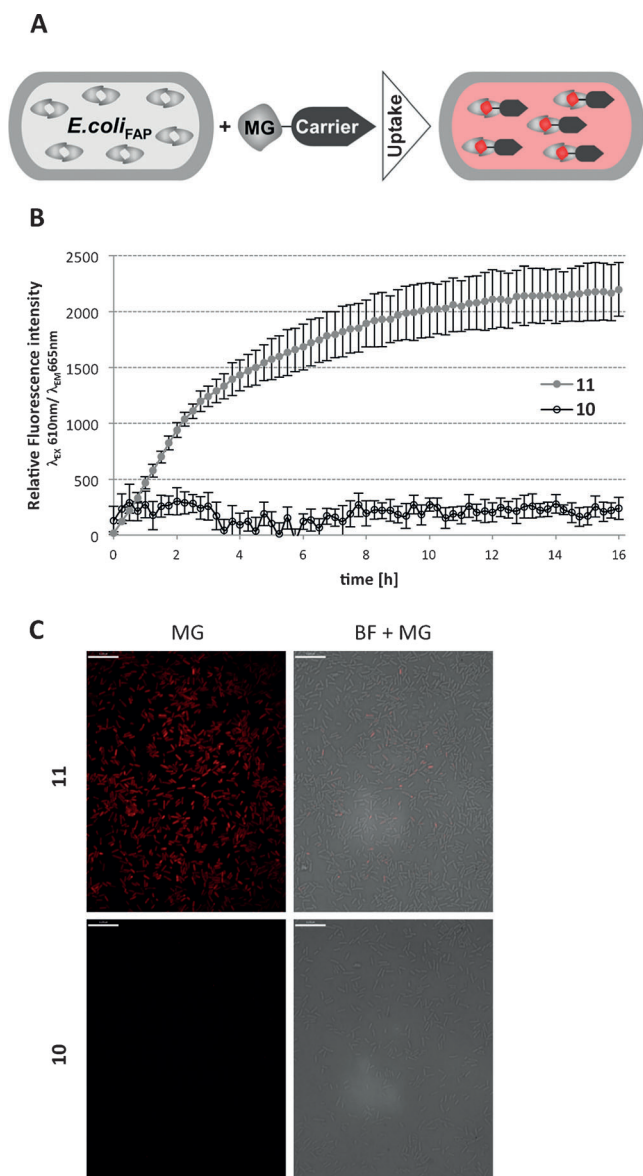


**Figure 3.** Monitoring uptake with the FAP system. a) Principle illustrating the application of the FAP system for uptake visualization of MG-carrier conjugates. b) **10** or **11** were added at a final concentration of  $10 \mu\text{M}$  to *E. coli*<sub>FAP6.2</sub>, and the fluorescence was recorded at  $\lambda_{EX}=610 \text{ nm}/\lambda_{EM}=665 \text{ nm}$  for 16 h. **11** was translocated to the cytoplasm, whereas **10** was not. c) Confocal microscopy images of *E. coli*<sub>FAP6.2</sub> upon incubation with  $10 \mu\text{M}$  **10** or **11** for 16 h. BF = bright field. Scale bars:  $11 \mu\text{m}$ .

The fluorescence intensity of **12** was highest at the site of bacterial injection after 0.6 h and decreased gradually; a clear signal was still visible after 5 h. In contrast, infected mice treated with **13** exhibited weaker signals. Uninfected mice treated with **12** gave rise to weaker intensities than the infected group. To visualize the site of infection by an independent method, type I interferon (IFN) production, as part of the immune response to bacterial infections, was localized by bioluminescence imaging 5 h post-injection, to account for the time lag associated with IFN induction. A strong bioluminescence signal co-localized with the fluores-

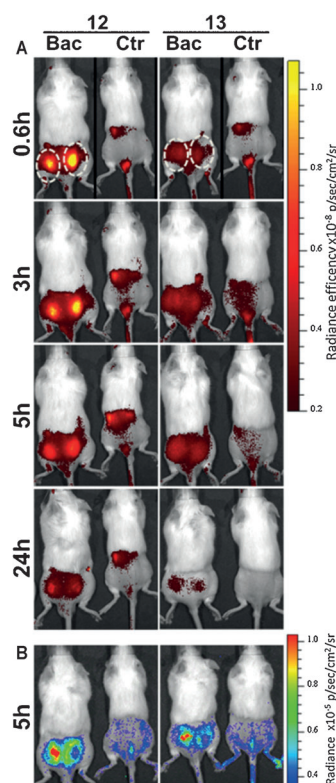


**Figure 4.** Small-animal model for the diagnosis of bacterial infections by siderophore conjugates. a) A suspension of bacteria (*P. aeruginosa* PAO1) was injected subcutaneously into the back (left and right) of interferon- $\beta$  luciferase reporter mice at the positions indicated by dashed white ovals (Bac), followed by intravenous injection of **12** or the control compound **13** into the tail vein. Uninfected animals (Ctr) were treated likewise. The fluorescence images were recorded after 0.6, 3, 5, and 24 h. b) A luciferin solution was injected intraperitoneally, and the animal bioluminescence induced by the host immune response was recorded after 5 h.

cence induced by **12**, thereby demonstrating that bacteria had not dissipated across the body, and that **12** correctly labeled the site of infection (Figure 4b). Thus a first proof of concept for the in vivo imaging of bacterial infections based on siderophore targeting has been demonstrated.

In summary, siderophore conjugates based on a DOTAM scaffold have been characterized as multifunctional agents that are applicable for the diagnosis and treatment of bacterial infections. Their ability to cross the Gram-negative cell wall was confirmed by microbiological experiments as well as by an adaptation of the FAP/MG system to *E. coli*, which encouraged the synthesis of antibiotic conjugates. Whereas the ampicillin conjugates **8** and **9** provided a first proof of concept for the use of the DOTAM scaffold as a carrier of antibiotics, we will attempt to improve the antibacterial activities by employing more potent effector molecules in next-generation conjugates. Additional future studies will be directed towards analogues with metal-bound DOTAM cores that may be suited for the detection of infections in larger animals.

## Conflict of interest

A patent that contains some of this work has been filed (see Ref. [10]).

**Keywords:** antibiotics · drug conjugates · drug delivery · imaging · siderophores

- [1] a) WHO in *Antimicrobial resistance: global report on surveillance*, WHO Press, **2014**; b) J. O'Neill in *Review on Antimicrobial Resistance*, **2014**, [https://amr-review.org/sites/default/files/AMR%20Review%20Paper%20-%20Tackling%20a%20crisis%20for%20the%20health%20and%20wealth%20of%20nations\\_1.pdf](https://amr-review.org/sites/default/files/AMR%20Review%20Paper%20-%20Tackling%20a%20crisis%20for%20the%20health%20and%20wealth%20of%20nations_1.pdf); c) H. W. Boucher, G. H. Talbot, J. S. Bradley, J. E. Edwards, D. Gilbert, L. B. Rice, M. Scheld, B. Spellberg, J. Bartlett, *Clin. Infect. Dis.* **2009**, *48*, 1–12; d) M. Bassetti, M. Merelli, C. Temperoni, A. Astilean, *Ann. Clin. Microbiol. Antimicrob.* **2013**, *12*, 22.
- [2] X. Wang, N. Murthy, *Sci. Transl. Med.* **2014**, *6*, 259fs243.
- [3] P. Panizzi, M. Nahrendorf, J. L. Figueiredo, J. Panizzi, B. Marinelli, Y. Iwamoto, E. Keliher, A. A. Maddur, P. Waterman, H. K. Kroh, F. Leuschner, E. Aikawa, F. K. Swirski, M. J. Pittet, T. M. Hackeng, P. Fuentes-Prior, O. Schneewind, P. E. Bock, R. Weissleder, *Nat. Med.* **2011**, *17*, 1142–1146.
- [4] a) X. Ning, S. Lee, Z. Wang, D. Kim, B. Stubblefield, E. Gilbert, N. Murthy, *Nat. Mater.* **2011**, *10*, 602–607; b) X. Ning, W. Seo, S. Lee, K. Takemiya, M. Rafi, X. Feng, D. Weiss, X. Wang, L. Williams, V. M. Camp, M. Eugene, W. R. Taylor, M. Goodman, N. Murthy, *Angew. Chem. Int. Ed.* **2014**, *53*, 14096–14101; *Angew. Chem.* **2014**, *126*, 14320–14325.
- [5] E. A. Weinstein, A. A. Ordonez, V. P. DeMarco, A. M. Murawski, S. Pokkali, E. M. MacDonald, M. Klunk, R. C. Mease, M. G. Pomper, S. K. Jain, *Sci. Transl. Med.* **2014**, *6*, 259ra146.
- [6] a) R. C. Hider, X. Kong, *Nat. Prod. Rep.* **2010**, *27*, 637–657; b) J. H. Crosa, A. R. Mey, S. M. Payne, *Iron transport in bacteria*, ASM Press, Washington, **2004**.
- [7] a) A. A. Lee, Y. S. Chen, E. Ekalestari, S. Y. Ho, N. S. Hsu, T. F. Kuo, T. A. Wang, *Angew. Chem. Int. Ed.* **2016**, *55*, 12338–12342; *Angew. Chem.* **2016**, *128*, 12526–12530; b) A. Kim, A. Kutschke, D. E. Ehmann, S. A. Patey, J. L. Crandon, E. Gorseth, A. A. Miller, R. E. McLaughlin, C. M. Blinn, A. Chen, A. S. Nayar, B. Dangel, A. S. Tsai, M. T. Rooney, K. E. Murphy-Benenato, A. E. Eakin, D. P. Nicolau, *Antimicrob. Agents Chemother.* **2015**, *59*, 7743–7752; c) P. Chairatana, T. Zheng, E. M. Nolan, *Chem. Sci.* **2015**, *6*, 4458–4471; d) A. Górska, A. Sloderbach, M. P. Marszall, *Trends Pharmacol. Sci.* **2014**, *35*, 442–449; e) M. G. Page, *Ann. N.Y. Acad. Sci.* **2013**, *1277*, 115–126; f) C. Ji, P. A. Miller, M. J. Miller, *J. Am. Chem. Soc.* **2012**, *134*, 9898–9901; g) C. Ji, R. E. Juárez-Hernández, M. J. Miller, *Future Med. Chem.* **2012**, *4*, 297–313; h) T. Zheng, J. L. Bullock, E. M. Nolan, *J. Am. Chem. Soc.* **2012**, *134*, 18388–18400; i) J. M. Roosenberg, Y. M. Lin, Y. Lu, M. J. Miller, *Curr. Med. Chem.* **2000**, *7*, 159–197.
- [8] a) M. Petrik, C. Zhai, H. Haas, C. Decristoforo, *Clin. Transl. Imaging* **2017**, *5*, 15–27; b) A. Szebesczyk, E. Olshvang, A. Shanzer, P. L. Carver, E. Gumienna-Kontecka, *Coord. Chem. Rev.* **2016**, *327–328*, 84–109; c) S. Noël, L. Guillon, I. J. Schalk, G. L. Mislin, *Org. Lett.* **2011**, *13*, 844–847; d) R. Nudelman, O. Ardon, Y. Hadar, Y. Chen, J. Libman, A. Shanzer, *J. Med. Chem.* **1998**, *41*, 1671–1678; e) H. Weizman, O. Ardon, B. Mester, J. Libman, O. Dwir, Y. Hadar, Y. Chen, A. Shanzer, *J. Am. Chem. Soc.* **1996**, *118*, 12368–12375.
- [9] S. S. Kelkar, T. M. Reineke, *Bioconjugate Chem.* **2011**, *22*, 1879–1903.
- [10] M. Broenstrup, H. Hu, G. Sergeev, WO2016026841A1, **2016**.
- [11] a) H. Y. Hu, N. H. Lim, D. Ding-Pfennigdorff, J. Saas, K. U. Wendt, O. Ritzeler, H. Nagase, O. Plettenburg, C. Schultz, M. Nazare, *Bioconjugate Chem.* **2015**, *26*, 383–388; b) L. M. De León-Rodríguez, Z. Kovacs, *Bioconjugate Chem.* **2008**, *19*, 391–402; c) F. Wojciechowski, M. Suchy, A. X. Li, H. A. Azab, R. Bartha, R. H. Hudson, *Bioconjugate Chem.* **2007**, *18*, 1625–1636.
- [12] G. J. Stasiuk, N. J. Long, *Chem. Commun.* **2013**, *49*, 2732–2746.
- [13] B. Schwyn, J. B. Neilands, *Anal. Biochem.* **1987**, *160*, 47–56.
- [14] a) N. Ohi, B. Aoki, T. Kuroki, M. Matsumoto, K. Kojima, T. Nehashi, *J. Antibiot.* **1987**, *40*, 22–28; b) U. Möllmann, L. Heinisch, A. Bauernfeind, T. Köhler, D. Ankel-Fuchs, *Biometals* **2009**, *22*, 615–624.
- [15] a) Q. Yan, S. L. Schwartz, S. Maji, F. Huang, C. Szent-Gyorgyi, D. S. Lidke, K. A. Lidke, M. P. Bruchez, *ChemPhysChem* **2014**, *15*, 687–695; b) C. Szent-Gyorgyi, B. F. Schmidt, Y. Creeger, G. W. Fisher, K. L. Zakel, S. Adler, J. A. Fitzpatrick, C. A. Woolford, Q. Yan, K. V. Vasilev, P. B. Berget, M. P. Bruchez, J. W. Jarvik, A. Waggoner, *Nat. Biotechnol.* **2008**, *26*, 235–240.
- [16] S. Saurabh, A. M. Perez, C. J. Comerci, L. Shapiro, W. E. Moerner, *J. Am. Chem. Soc.* **2016**, *138*, 10398–10401.

Manuscript received: February 7, 2017

Revised manuscript received: April 4, 2017

Version of record online: ■■■■■■, ■■■■■■

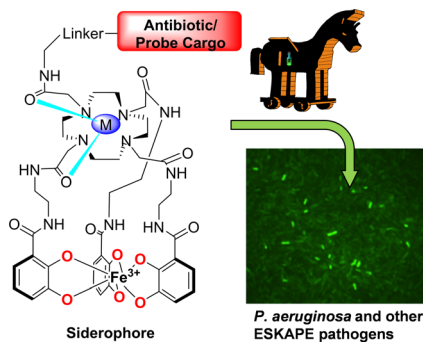
## Communications



## Antibiotic Conjugates

K. Ferreira, H.-Y. Hu, V. Fetz,  
H. Prochnow, B. Rais, P. P. Müller,  
M. Brönstrup\*      

Multivalent Siderophore–DOTAM  
Conjugates as Theranostics for Imaging  
and Treatment of Bacterial Infections



**Trojan horses:** A siderophore motif was coupled to functional imaging and/or antibiotic moieties via a DOTAM scaffold. The conjugates are internalized into Gram-positive as well as Gram-negative pathogenic bacteria and can be used for multiple theranostic applications, such as the in vivo imaging of infections.